Multiple one-electron oxidation and reduction of trinuclear bis(2,4-pentanedionato)ruthenium complexes with substituted diquinoxalino[2,3-*a*:2′,3′-*c*]phenazine ligands

Sandeep Ghumaan [a], Biprajit Sarkar [b], Mahendra P. Patil [a], Jan Fiedler [c], Raghavan B. Sunoj [a,*], Wolfgang Kaim [b,*], Goutam Kumar Lahiri [a,*]

[a] *Department of Chemistry, Indian Institute of Technology – Bombay, Powai, Mumbai 400076, India*
[b] *Institut für Anorganische Chemie, Universität Stuttgart, Pfaffenwaldring 55, D – 70550 Stuttgart, Germany*
[c] *J. Heyrovský Institute of Physical Chemistry, v.v.i., Academy of Sciences of the Czech Republic, Dolejškova 3, CZ – 18223 Prague, Czech Republic*

Abstract

The complexes (μ_3-L^1/L^2)[Ru(acac)$_2$]$_3$, acac$^-$ = 2,4-pentanedionato, L^1 = 2,3,8,9,14,15-hexachlorodiquinoxalino[2,3-*a*:2′,3′-*c*]phenazine and L^2 = 2,3,8,9,14,15- hexamethyldiquinoxalino[2,3-*a*:2′,3′-*c*]phenazine, undergo stepwise one-electron oxidation involving a total of three electrons and stepwise one-electron reduction with three (L^2) or four electrons (L^1). All reversibly accessible states were characterized by UV–Vis–NIR spectroelectrochemistry. Oxidation leads to mixed-valent intermediates $\{(\mu_3\text{-L})[Ru(acac)_2]_3\}^+$ and $\{(\mu_3\text{-L})[Ru(acac)_2]_3\}^{2+}$ of which the $Ru^{III}Ru^{II}Ru^{II}$ combinations exhibit higher comproportionation constants K_c than the $Ru^{III}Ru^{III}Ru^{II}$ states – in contrast to a previous report for the unsubstituted parent systems $\{(\mu_3\text{-}L^3)[Ru(acac)_2]_3\}^{+/2+}$, L^3 = diquinoxalino[2,3-*a*:2′,3′-*c*]phenazine. No conspicuous inter-valence charge transfer absorptions were observed for the mixed-valent intermediates in the visible to near-infrared regions. The monocations and monoanions were characterized by EPR spectroscopy, revealing rhombic ruthenium(III) type signals for the former. Electron addition produces ruthenium(II) complexes of the reduced forms of the ligands L, a high resolution EPR spectrum with ^{14}N and ^{35,37}Cl hyperfine coupling and negligible *g* anisotropy was found for $\{(\mu_3\text{-}L^1)[Ru(acac)_2]_3\}^-$. DFT calculations of ($\mu_3$-$L^1$)[Ru(acac)$_2$]$_3$ confirm several ligand-centered low-lying unoccupied MOs for reduction and several metal-based high-lying occupied MOs for electron withdrawal, resulting in low-energy metal-to-ligand charge transfer (MLCT) transitions.

Keywords: DFT calculations; EPR; Radical complexes; Ruthenium; Electrochemistry; Spectroelectrochemistry

1. Introduction

In contrast to the vast number of mixed-valent ligand-bridged diruthenium complexes [1] there have been relatively few reports on the electron transfer reactivity of symmetrically trinuclear compounds [2–8]. If the common Ru^{III}/Ru^{II} redox pairs are involved, this arrangement leads to two homovalent and to two different mixed-valent states, the odd-electron form $Ru^{III}Ru^{II}Ru^{II}$ and the even-electron species $Ru^{III}Ru^{III}Ru^{II}$. Electron transfer to or from a trigonally symmetrical system can involve partial occupation of degenerate orbitals with the resulting tendency for distortion.

Following a previous report [8] on the synthesis and spectroelectrochemical characterization of unsubstituted (μ_3-L^3)[Ru(acac)$_2$]$_3$ (**3**), a trinuclear complex of the extended π ligand L^3 = diquinoxalino[2,3-*a*:2′,3′-*c*]phenazine, we now describe the results for the redox systems $\{(\mu_3\text{-}L^1)[Ru(acac)_2]_3\}^n$, $\mathbf{1}^n$, and $\{(\mu_3\text{-}L^2)[Ru(acac)_2]_3\}^n$, $\mathbf{2}^n$, with the hexasubstituted ligands L^1 and L^2 (Scheme 1).

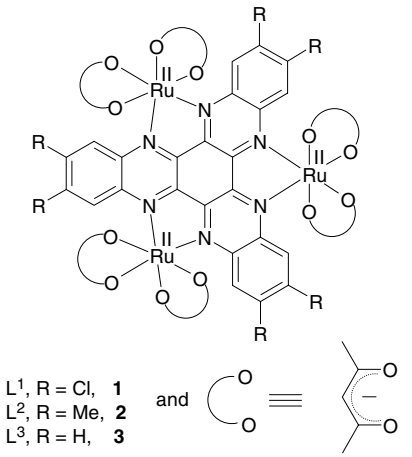

Scheme 1.

DFT calculation results are reported for the hexachloro-substituted **1**, involving structure optimization and MO description. Voltammetric methods were employed to establish multistep reversible electron transfer while spectroelectrochemistry in the UV–Vis–NIR region as well as EPR in the X band (9.5 GHz) were used to characterize the intermediates.

2. Experimental

2.1. Materials

The precursor compounds $Ru(acac)_2(CH_3CN)_2$ [9], 2,3,8,9,14,15-hexachlorodiquinoxalino[2,3-*a*:2′,3′-*c*]phenazine (L^1) [10] and 2,3,8,9,14,15-hexamethyldiquinoxalino[2,3-*a*:2′,3′-*c*]phenazine (L^2) [11][1] were prepared according to the reported procedures. Other chemicals and solvents were reagent grade and used as received. For spectroscopic and electrochemical studies HPLC grade solvents were used.

2.2. Physical measurements

UV–Vis–NIR spectroelectrochemical studies were performed in CH_3CN/0.1 M Bu_4NPF_6 at 298 K using an optically transparent thin layer electrode (OTTLE) cell [12] in connection with a J&M TIDAS spectrophotometer. FT-IR spectra were taken on a Nicolet spectrophotometer with samples prepared as KBr pellets. Solution electrical conductivity was checked using a Systronic 305 conductivity bridge. ^{1}H NMR spectra were obtained with a 400 MHz Varian FT spectrometer. The EPR measurements were made in a two-electrode capillary tube [13] with an X-band Bruker system ESP300, equipped with a Bruker ER035M gaussmeter and a HP 5350B microwave counter. Cyclic voltammetric, differential pulse voltammetric and coulometric measurements were carried out using a PAR model 273A electrochemistry system. Platinum wire working and auxiliary electrodes and an aqueous saturated calomel reference electrode (SCE) were used in a three-electrode configuration. The supporting electrolyte was 0.1 M Et_4NClO_4 and the solute concentration was $\sim 10^{-3}$ M. The half-wave potential E°_{298} was set equal to $0.5(E_{pa} + E_{pc})$, where E_{pa} and E_{pc} are the anodic and cathodic cyclic voltammetric peak potentials, respectively. A platinum wire-gauze working electrode was used in the coulometric experiments. The elemental analysis was carried out with a Perkin–Elmer 240C elemental analyzer. Electrospray mass spectra were recorded on a Micromass Q-ToF mass spectrometer.

2.3. Preparation of complexes *1* and *2*

2.3.1. $[\{(acac)_2Ru^{II}\}_3(\mu\text{-}L^1)]$ (*1*)

The starting complex $Ru(acac)_2(CH_3CN)_2$ (100 mg, 0.26 mmol) and the ligand L^1 (52 mg, 0.087 mmol) were added to 20 ml of ethanol, and the mixture was heated to reflux for 6 h under a dinitrogen atmosphere. The initial orange solution gradually changed to dark green. The solvent was evaporated to dryness and the residue was purified by using a silica gel column. Initially, a red compound corresponding to $Ru(acac)_3$ was eluted by CH_2Cl_2–CH_3CN (25:1 v/v). With CH_2Cl_2–CH_3CN (20:1 v/v), a green compound corresponding to **1** was then separated. Yield: 45 mg, 35%. *Anal.* Calc. for $C_{54}H_{48}Cl_6N_6O_{12}Ru_3$: C, 43.55; H, 3.25; N, 5.65. Found: C, 43.20; H, 3.10; N, 5.32%. ^{1}H NMR (400 MHz) in $(CD_3)_2SO$ δ (ppm), 8.29/8.27, 8.21/8.19 (s, (CH(L^1)), 5.67/5.66/5.64 (s, CH(acac)), 2.34; 1.68/1.67 (s, CH_3(acac)). The positive ion electrospray mass spectrum of **1** shows the molecular ion peak centered (*m*/*z*) at 1489.58, corresponding to $\mathbf{1}^+$ (calculated molecular mass, 1488.94) and a peak centered (*m*/*z*) at 1388.53 corresponding to $\{\mathbf{1}\text{-acac}\}^+$ (calculated molecular mass, 1389.83).

2.3.2. $[\{(acac)_2Ru^{II}\}_3(\mu\text{-}L^2)]$ (*2*)

The complex $Ru(acac)_2(CH_3CN)_2$ (100 mg, 0.26 mmol) and L^2 (41 mg, 0.087 mmol) were added to 20 ml of ethanol and the mixture was heated to reflux for 12 h under a dinitrogen atmosphere. The initial orange solution gradually changed to bluish green. The solvent was evaporated and the residue purified by using a silica gel column. Initially, a red compound corresponding to $Ru(acac)_3$ was eluted by CH_2Cl_2–CH_3CN (25:1 v/v). With CH_2Cl_2–CH_3CN (5:1 v/v), a blue compound corresponding to **2** was separated. Yield: 55 mg, 46%. *Anal.* Calc. for $C_{60}H_{66}N_6O_{12}Ru_3$: C, 52.62; H, 4.86; N, 6.14. Found: C, 52.83; H, 4.85; N, 6.22%. ^{1}H NMR (400 MHz) in $(CD_3)_2SO$ δ (ppm), 8.34/8.28; 8.15/7.94 (s, CH(L^2)), 5.76/5.52 (s, CH(acac)), 2.41/2.21/1.56 (multiplet, CH_3). The positive ion electrospray mass spectrum of **2** shows the molecular ion peak centered (*m*/*z*) at 1365.95, corresponding to $\mathbf{2}^+$ (calculated molecular mass, 1366.43).

[1] The heterocyclic system was referred to as 5,6,11,12,17,18-hexaazatrinaphthalene (Ref. [11]).

2.4. Computational details

Complete geometry optimization without symmetry constraints was carried out for **1** in the Δ_3/Λ_3 configuration, using the density functional theory method at the B3LYP level. The Δ_3/Λ_3 configuration was chosen for convenience, isomerism was shown to affect the electronic structure very little [1f,1i,1j,3]. All elements except ruthenium were assigned a 6-31G* basis set. The Stuttgart–Dresden effective core potential (ECP), representing 19 core electrons, along with valence basis sets (SDD) was used for the ruthenium atoms [14a,14b]. Calculations were performed with GAUSSIAN 98 [14c]. Vertical electronic excitations based on B3LYP optimized geometries were computed using the time-dependent density functional theory (TD-DFT) formalism [14d,14e] with the B3LYP functional using the above combination of basis sets. Extinction coefficients were obtained from calculated oscillator strengths using Gaussian line shape and a full width at half maximum (fwhm) of 0.4 eV = 3228 cm^{-1} [14f]. The molecular orbital compositions have been determined using the programme AOMIX using the B3LYP/SDD,6-31G* wave function [14g]. Visual inspection of all key orbitals was done with MOLDEN [14h] to assign the nature of various electronic transitions.

3. Results and discussion

Regardless of the molar ratio of the reactants, the trinuclear complexes **1** and **2** were invariably obtained from reactions between $Ru(acac)_2(CH_3CN)_2$ and either of the free ligands. The well established [9,15] π electron donor capacity of the $Ru^{II}(acac)_2$ complex fragment is held responsible for enhancing the metal affinity of mono- and dinuclear intermediates through extensive π conjugation until full charge transfer supported coordinative saturation [16] is achieved.

Positive ion electrospray mass spectroscopy of **1** (Fig. 1a) and **2** (Fig. 1b) support the identity of the new hexasubstituted complexes. The ^1H NMR spectra of **1** and **2** exhibit two sets of signals both for the aromatic CH protons of L^1 and L^2 and for the CH/CH_3 groups of the $acac^-$ ligands (Fig. 2, Section 2). The presence of two sets of signals in each case indicates the existence of mixtures of two diastereoisomers (Δ_3/Λ_3 or $\Delta_2\Lambda/\Lambda_2\Delta$) in solution. The two closely spaced singlets for all protons involved with a particular diastereoisomeric form result from the pseudo C_3-symmetry of the molecule. In related cases such isomerism was shown to affect the electrochemical and spectroscopic response only slightly [1f,1i,1j,3], we therefore used the product distributions as obtained and as characterized by NMR (Fig. 2).

Full geometry optimization of complex **1** in the Δ_3/Λ_3 configuration was carried out at the B3LYP level of theory by using the SDD basis set for Ru and the 6-31G* basis for all other atoms (Fig. 3). Important optimized structural parameters of complex **1** are summarized in Tables S1

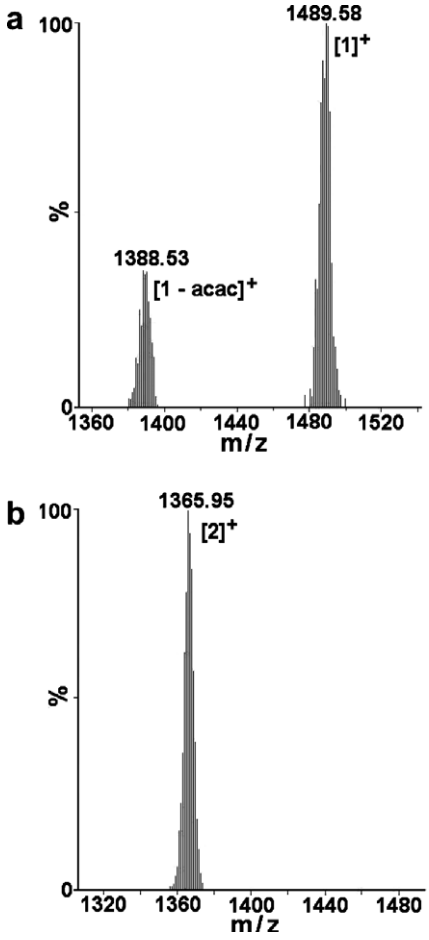

Fig. 1. Electrospray mass spectra of: (a) **1** and (b) **2** in CH_3CN.

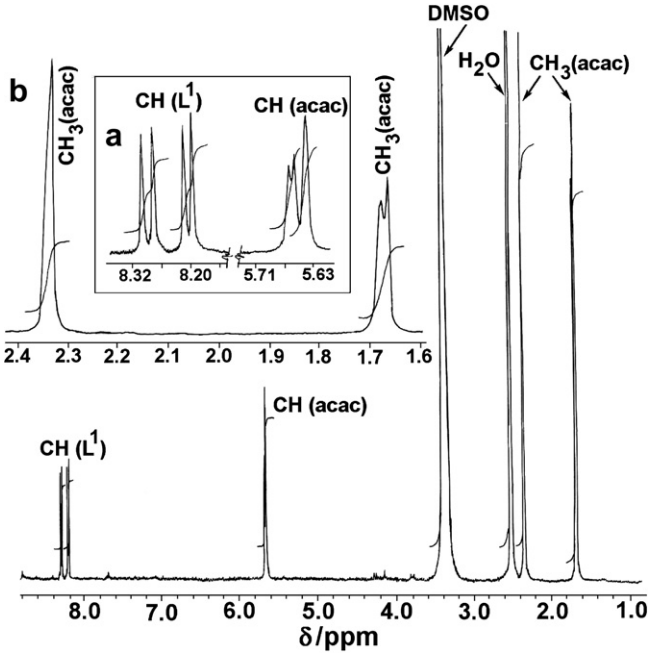

Fig. 2. ^1H NMR spectrum of **1** in $(CD_3)_2SO$. Inserts show expanded parts of the spectrum in the range of: (a) 5.5–8.5 ppm and (b) 1.5–2.5 ppm.

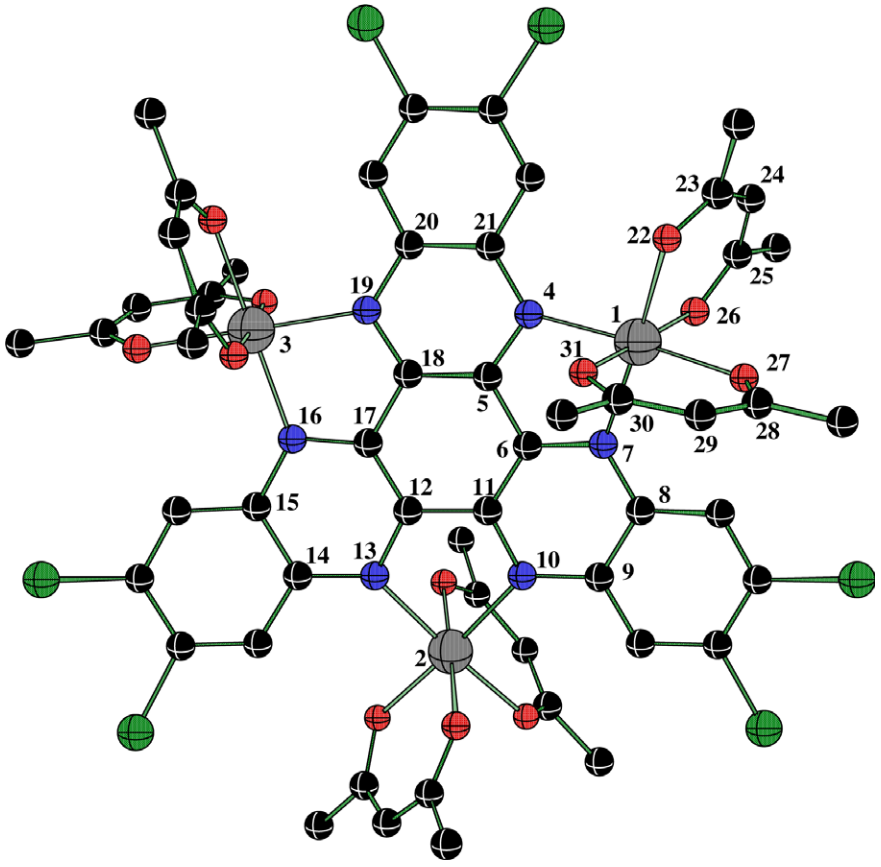

Fig. 3. Optimized structure of complex **1** at the B3LYP level of theory by using the SDD basis set for Ru and 6-31G* for all other atoms (no symmetry constraints).

and S2. The Ru–N and Ru–O(acac) distances are found to vary only slightly and range between 2.06 and 2.08 Å. The N(4)–C(5) and N(7)–C(6) π bonds are found to be elongated by about 0.023 Å in **1** as compared to the free ligand L^1, and this N–C π bond elongation is nearly the same at each ruthenium center which signifies the comparable extent of π back-bonding from each Ru^{II} ion (*vide infra*). The metal centers were found to be separated by about 6.9 Å (Table S1).

Electrochemically the complexes **1** and **2** exhibit multiple reversible one-electron reduction waves which are associated with the highly conjugated bridging ligands (L^1/L^2); the potentials also vary systematically with the electronic nature of the substituents, Me or Cl. In case of **1**, four distinct reduction processes were observed whereas only three waves were detected for **2** (Table 1, Fig. 4). In addition, **1** and **2** display three successive oxidation processes corresponding to the reversible transitions $Ru^{II}Ru^{II}Ru^{III} \rightleftharpoons Ru^{II}Ru^{II}Ru^{II}$ (couple I), $Ru^{II}Ru^{III}Ru^{III} \rightleftharpoons Ru^{II}$ $Ru^{II}Ru^{III}$ (couple II), and $Ru^{III}Ru^{III}Ru^{III} \rightleftharpoons Ru^{II}Ru^{III}Ru^{III}$ (couple III) (Table 1, Fig. 4). These potentials are lower for R = Me (complex **2**) than for R = Cl (complex **1**) (Table 1), as expected from the different electron donating and withdrawing abilities. Remarkably, the separation between the redox potentials for complex oxidation leads to larger comproportionation

Table 1
Electrochemical data[a]

Compound	E°_{298}/V(ΔE_p, mV)						
	Couples						
	I	II	III	IV	V	VI	VII
1	0.16 (70)	0.56 (70)	0.79 (90)	−0.84 (70)	−0.98 (70)	−1.23 (80)	−1.71 (90)
2	0.01 (60)	0.41 (90)	0.62 (70)	−1.09 (60)	−1.20 (80)	−1.58 (100)	
3[b]	0.34 (70)	0.68 (70)	1.16 (70)	−0.46 (80)	−1.07 (70)	−1.61 (80)	

[a] In CH_3CN/0.1 M Et_4NClO_4 vs. SCE. ΔE_p: peak potential difference.
[b] Ref. [8].

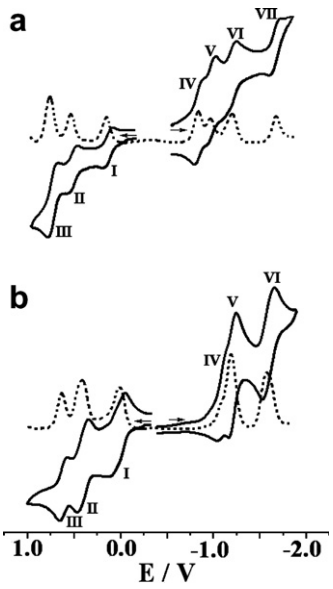

Fig. 4. Cyclic voltammograms (—) and differential pulse voltammograms (---) in CH_3CN/0.1 M Et_4NClO_4 of: (a) **1** and (b) **2**; potentials against SCE.

constants for the first intermediate (K_{c1}) than for the second form, $Ru^{II}Ru^{III}Ru^{III}$ (K_{c2}), both for $\mathbf{1}^{n+}$ and $\mathbf{2}^{n+}$, respectively ($RT\ln K_c = nF(\Delta E)$ [1]). Usually, the opposite is observed (Table 2) due to increasing Coulombic interactions; for instance, K_c values for the corresponding parent complex $\mathbf{3}^{n+}$ with R = H have been reported at $10^{5.7}$ (K_{c1}) < $10^{8.0}$ (K_{c2}). In comparison to $\mathbf{3}^{n}$ K_{c1} appears to be slightly greater for $\mathbf{1}^{n+}$ or $\mathbf{2}^{n+}$, however, K_{c2} is much larger for $\mathbf{3}^{n+}$ than for $\mathbf{1}^{n+}$ or $\mathbf{2}^{n+}$.

The electrolyte-dependent [17a,17b] comproportionation constants K_c reflect several different effects such as the electrostatic interaction, an inductive factor, the resonance exchange, the antiferromagnetic exchange stabilization, and ion-pairing effects [17c,17d,17e]. Their comparative interpretation is thus not always as straightforward as commonly believed. In the present case, the smaller range for the dicationic, i.e. rather highly charged $Ru^{II}Ru^{III}Ru^{III}$ forms may reflect diminished Coulombic effects due to enhanced charge delocalization by the six π donating Cl ($\mathbf{1}^{2+}$) or inductively electron donating Me substituents ($\mathbf{2}^{2+}$). Not unexpectedly, the potentials for corresponding diastereoisomers are rather similar [3,18,19]. Nevertheless, the profile of the cyclic voltammograms, in particular for **2**, suggests the existence of two diastereoisomers in solution as has also been observed by ^{1}H NMR (Fig. 2, Section 2).

The EPR spectra taken of monocations and monoanions are in agreement with expectations [8] for the frontier orbital situation and with the DFT calculated orbital

Table 2
The variation of K_c and IVCT values in symmetrical triruthenium complexes

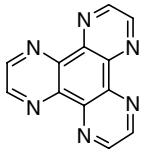

L^4

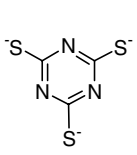

L^5

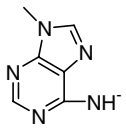

L^6

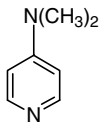

dmap

Formula	K_{c1}[a]	K_{c2}[a]	$(IVCT)_1$[b]	$(IVCT)_2$[b]	Ref.
			λ (nm) (ε, M^{-1} cm^{-1})	λ (nm) (ε, M^{-1} cm^{-1})	
$[\{(acac)_2Ru\}_3(\mu_3\text{-}L^1)]$ (**1**)	$10^{6.8}$	$10^{3.9}$	[c]	[c]	this work
$[\{(acac)_2Ru\}_3(\mu_3\text{-}L^2)]$ (**2**)	$10^{6.8}$	$10^{3.6}$	[c]	[c]	this work
$[\{(acac)_2Ru\}_3(\mu_3\text{-}L^3)]$ (**3**)	$10^{5.7}$	$10^{8.1}$	[c]	[c]	[8]
Δ_3/Λ_3-$[\{(bpy)_2Ru\}_3(\mu_3\text{-}L^4)]^{6+}$	$10^{3.9}$	$10^{4.1}$	2150 (3315)	2130 (2990)	[3b]
$\Delta_2\Lambda/\Lambda_2\Delta$-$[\{(bpy)_2Ru\}_3(\mu_3\text{-}L^4)]^{6+}$	$10^{3.7}$	$10^{4.1}$	2155 (4180)	2236 (2150)	[3b]
$[\{(phen)_2Ru\}_3(\mu_3\text{-}L^4)]^{6+}$	$10^{4.5}$	$10^{4.7}$	[c]	[c]	[3d]
$[\{(bpy)_2Ru\}_3(\mu_3\text{-}L^5)]^{3+}$	$10^{3.7}$	$10^{4.1}$	1900 (2300)	1900 (2400)	[4]
$[\{(phen)_2Ru\}_3(\mu_3\text{-}L^5)]^{3+}$	$10^{3.2}$	$10^{4.1}$	[d]	[d]	[4]
$[\{(pap)_2Ru\}_3(\mu_3\text{-}L^5)]^{3+}$	10^{20}	$10^{3.4}$	[d]	[d]	[5]
$[\{([9]\text{-ane-}S_3)Ru(\mu\text{-}L^6)\}_3]^{3+}$	$10^{3.0}$	$10^{6.4}$	950 (2950)	2085 (8400)	[6,7]
$[Ru_3(O)(CH_3CO_2)_6(CO)(dmap)_2]$	10^{16}	10^{27}	[d]	[d]	[2]
$[Ru_3(O)(CH_3CO_2)_6(CO)(py)_2]$	$10^{14.6}$	10^{26}	[d]	[d]	[2]
$[Ru_3(O)(CH_3CO_2)_6(CO)(CNXy)_2]$	$10^{10.2}$	10^{14}	[d]	[d]	[2]
$[Ru_3(O)(CH_3CO_2)_6(CNXy)(py)_2]$	$10^{13.5}$	10^{21}	[d]	[d]	[2]
$[Ru_3(O)(CH_3CO_2)_6(CNXy)_2(py)]$	10^{18}	10^{13}	[d]	[d]	[2]
$[Ru_3(O)(CH_3CO_2)_6(CNXy)_2(dmap)]$	10^{22}	10^{13}	[d]	[d]	[2]
$[Ru_3(O)(CH_3CO_2)_6(CNXy)_3]$	$10^{8.8}$	10^{11}	1004 (12200)	1002 (6400)	[2]

[a] K_c: comproportionation constant for $Ru_3^{III,II,II}$(K_{c1}) and $Ru_3^{III,III,II}$(K_{c2}).
[b] IVCT: inter-valence charge-transfer transitions for the $Ru_3^{II,II,III}$($IVCT_1$) and $Ru_3^{II,III,III}$ states ($IVCT_2$).
[c] Not observed.
[d] Not reported.

compositions (see Table 4). The cations exhibit rhombic Ru^{III} type signals with considerable g anisotropy in the immobilized state (Fig. 5, Table 3); this and the average g above 2 are indicative of low-spin d^5 species in a distorted octahedral situation [20].

In contrast, the monoanions exhibit EPR features without detectable g anisotropy at X band frequency (9.5 GHz), the isotropic g values near 2.00 (Table 3) signify vanishing participation of atoms with large spin–orbit coupling constants at the spin distribution [21]. The complex anion $\mathbf{1}^{\cdot-}$ was even found to exhibit hyperfine structure caused by coupling with ^{14}N ($I = 1$) and $^{35,37}Cl$ nuclei ($I = 3/2$) at the order of about 1 G (Fig. 6). These values are compatible with the composition of the lowest unoccupied MO (see Fig. 8), small, unresolved hyperfine interaction with the total of 18 methyl hydrogen atoms is likely to obscure the hyperfine structure for $\mathbf{2}^{\cdot-}$. Evidence for symmetry lowering on the EPR time scale has not been observed, there is probably rapid equilibration of any distortions.

The signal detectability at room temperature, the small line-width allowing for EPR resolution, the isotropic g factors close to the free electron value of 2.0023, and the absence of metal ($^{99,101}Ru$, $I = 5/2$) hyperfine splitting and of g anisotropy at 9.5 GHz are all in agreement with an almost exclusively ligand-centered spin [21]. In fact, the results suggest much less metal participation than in complexes of $[Ru(bpy)_2]^{2+}$ with anion radical ligands [13], probably because of the donor characteristics of $Ru(acac)_2$ in comparison to $[Ru(bpy)_2]^{2+}$.

The energies and the composition of the frontier Kohn–Sham orbitals (Figs. 7 and 8) have been examined using the AOMIX programme [14g,22]. The filled levels (between HOMO and HOMO − 6) are predominantly metal-centered orbitals with total Ru contributions of around 65% and additional mixing with the π orbitals of $acac^-$ (Table 4). The unfilled levels, on the other hand, are primarily located over the L^1 unit, having π^*

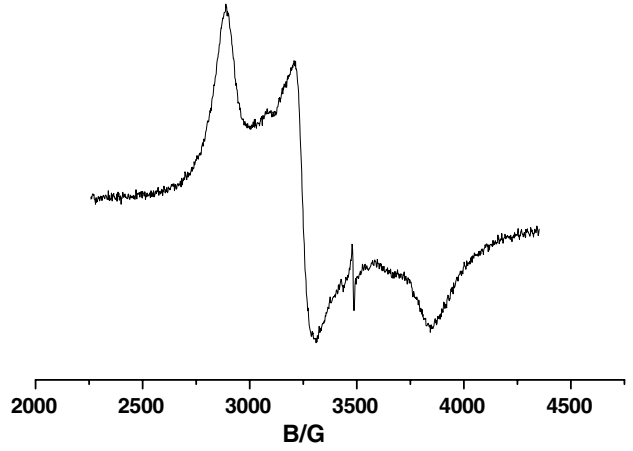

Fig. 5. EPR spectrum of $\mathbf{2}^+$ in CH_3CN/0.1 M Bu_4NPF_6 at 4 K (artefact radical signal from cavity at 3500 G).

Table 3
EPR data of monocations and monoanions

Compound	g_1	g_2	g_3	g_{iso}	Δg	Ref.
$\mathbf{1}^{\cdot-}$	[a]	[a]	[a]	2.0053	<0.10	this work
$\mathbf{1}^+$	2.398	2.140	1.815	2.131[b]	0.583	this work
$\mathbf{2}^{\cdot-}$	[a]	[a]	[a]	1.9706	<0.10	this work
$\mathbf{2}^+$	2.370	2.107	1.782	2.100[b]	0.589	this work
$\mathbf{3}^{\cdot-}$	2.058	2.058	1.924	1.969[b]	0.133	[8]
$\mathbf{3}^+$	2.332	2.154	1.877	2.128[b]	0.455	[8]

[a] Not resolved.
[b] g_{av} (calculated).

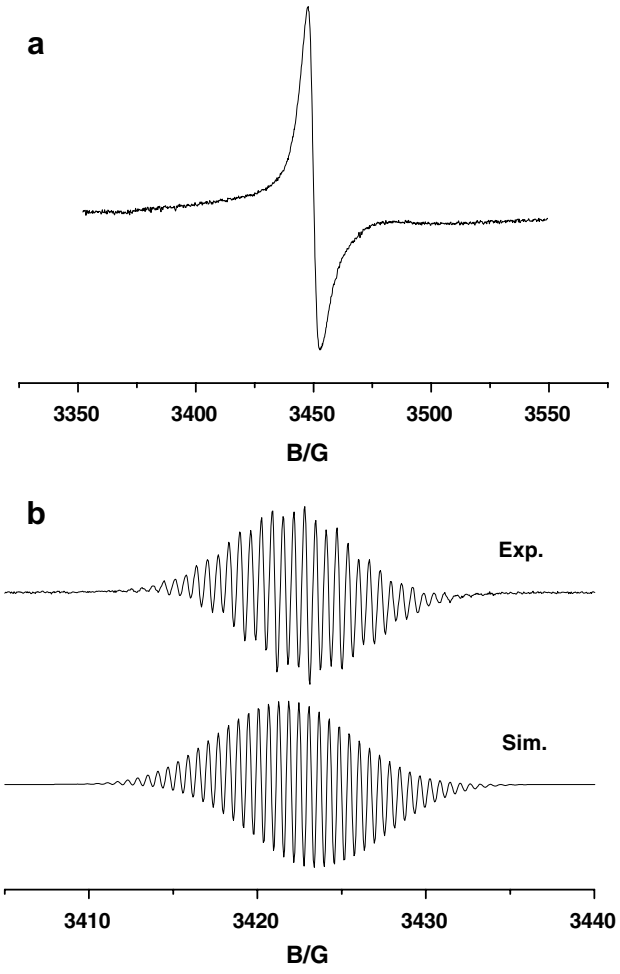

Fig. 6. EPR spectra of $\mathbf{1}^-$ at: (a) 110 K and (b) 298 K (top: experimental, bottom: simulated) in CH_3CN/0.1 M Bu_4NPF_6. Simulation parameters 1.8 G ($6\times{}^{14}N$) and 0.6/0.5 G ($6\times{}^{35}Cl/{}^{37}Cl$ in natural abundance).

characteristics[2]. Atomic orbital contributions from the metal centers towards the LUMO are successfully adopted in explaining the back-bonding within metal complexes in more quantitative fashion [23]. In the present case, the con-

[2] We have identified the π^* orbital of L^1 as the one in the xy-plane by careful analysis of the MO coefficient of the LUMO, which is mainly located on π^* of L^1 (66%) with minor contribution from dπ on Ru. Further, the d-orbital in the same plane as that of L^1 is taken as the d_{xy} and the remaining orthogonal d-orbitals as d_{xz} and d_{yz}.

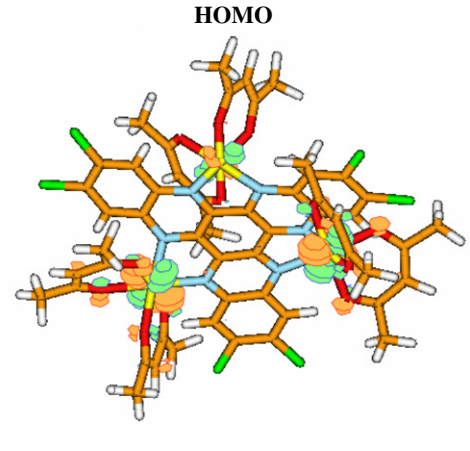

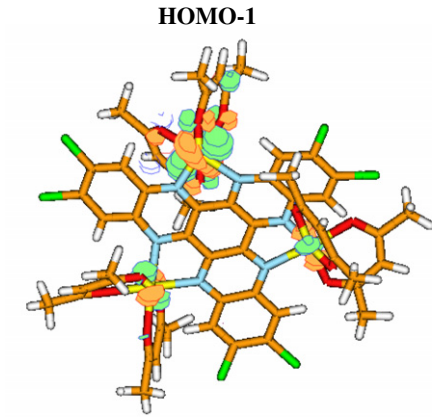

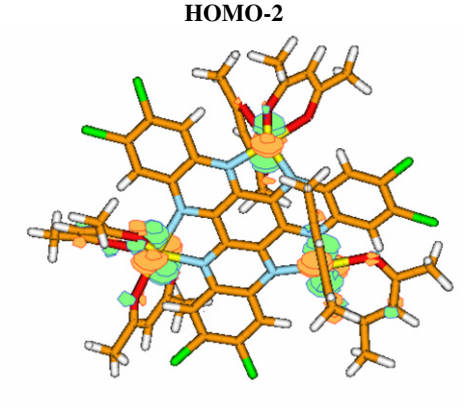

Fig. 7. Representative orbital contour diagrams of the HOMOs of **1**.

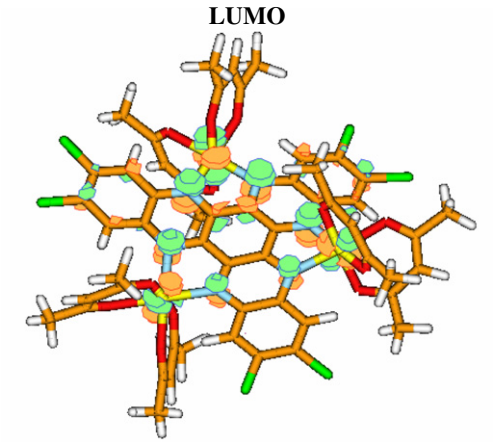

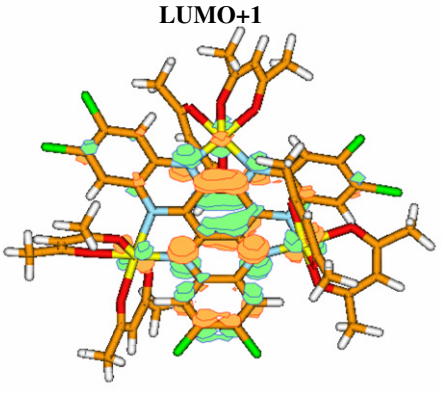

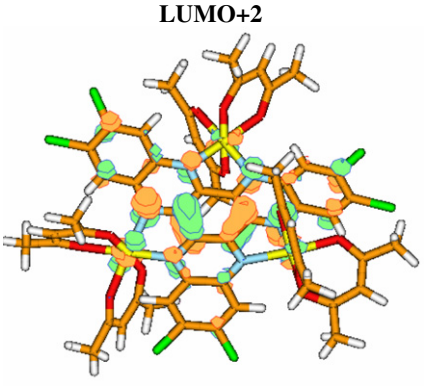

Fig. 8. Representative orbital contour diagrams of the LUMOs of **1**.

Table 4
Orbital energies and atomic orbital contributions for the frontier molecular orbitals of **1** computed without symmetry constraints

MO	Orbital energy (eV)	%Ru1	%Ru2	%Ru3	$\%Ru_{total}$	$\%L^1$	%acac
LUMO + 2	−2.95 (23790)[a]	6.5	4.6	2.9	14.0	82.7	3.3
LUMO + 1	−2.96 (23870)	5.2	6.7	3.9	15.8	81.3	2.9
LUMO	−3.16 (25490)	8.1	8.4	12.2	28.7	66.1	5.3
HOMO	−4.86 (39200)	29.1	30.3	6.5	65.9	7.2	26.9
HOMO − 1	−4.91 (39600)	10.7	8.2	47.1	66.0	5.3	29.7
HOMO − 2	−4.98 (40170)	25.5	26.6	16.1	68.2	6.6	25.2

[a] Values in parentheses indicate orbital energy in cm^{-1}.

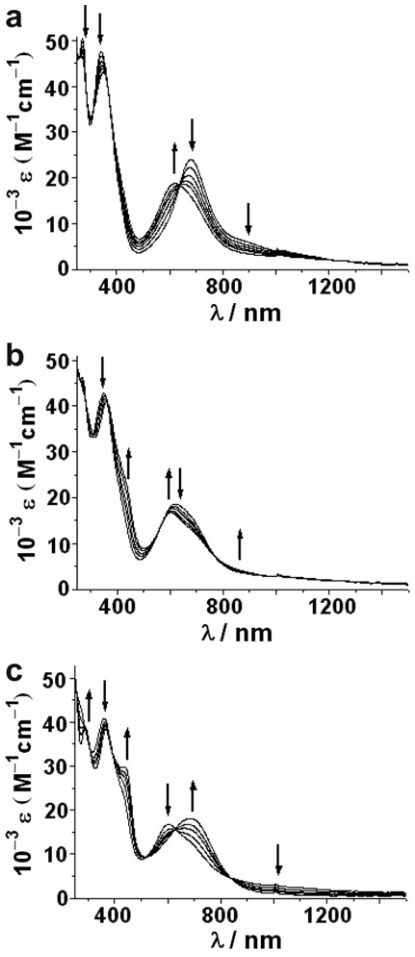

Fig. 9. UV–Vis–NIR spectroelectrochemistry for the conversions: (a) $\mathbf{1} \rightarrow \mathbf{1}^{+}$, (b) $\mathbf{1}^{+} \rightarrow \mathbf{1}^{2+}$ and (c) $\mathbf{1}^{2+} \rightarrow \mathbf{1}^{3+}$in CH_3CN/0.1 M Bu_4NPF_6.

tributions from the ruthenium atoms towards the LUMO are found to be about the same on average, the effective trigonal symmetrical situation being further confirmed by the optimized geometrical parameters around the ruthenium atoms. Nonetheless, the metals contribution especially to the calculated LUMO seems to be overestimated, considering the EPR results with their suggestion of marginal ruthenium influence.

UV–Vis–NIR absorption spectroelectrochemistry was performed for the multistep series $\mathbf{1}^{3+}$–$\mathbf{1}^{4-}$ (Figs. 9 and 10) and $\mathbf{2}^{3+}$–$\mathbf{2}^{3-}$ (Table 5).

The results show similar trends for both series in agreement with the donor effect of both kinds of substituents. The free ligands have long-wavelength π–π* absorption bands at about 412 nm (ε ca. $6 \times 10^4\ M^{-1}\,cm^{-1}$) whereas the lowest energy absorption maxima of **1** and **2** lie around 660 nm (ε ca. $1.8 \times 10^4\ M^{-1}\,cm^{-1}$). These bands are assumed to derive from allowed metal-to-ligand charge transfer (MLCT) transitions, given by the experimentally and computationally suggested presence of several high-lying occupied d levels and low-lying unoccupied ligand π* orbitals.

A selected list of computed vertical excitation energies using the time-dependent density functional theory (TD-DFT) is therefore given in Table S2. For **1**, two transitions with fairly high oscillator strengths and calculated extinction coefficients have been obtained, one at 781 nm ($\varepsilon = 2914\ M^{-1}\,cm^{-1}$) and another at 771 nm ($\varepsilon = 4993\ M^{-1}\,cm^{-1}$). The quantitative assessment of these orbital overlap-favored MLCT processes compares with experimental values for **1** of 890 nm(sh) and 680 nm ($\varepsilon = 23\,900\ M^{-1}\,cm^{-1}$). As must be expected for

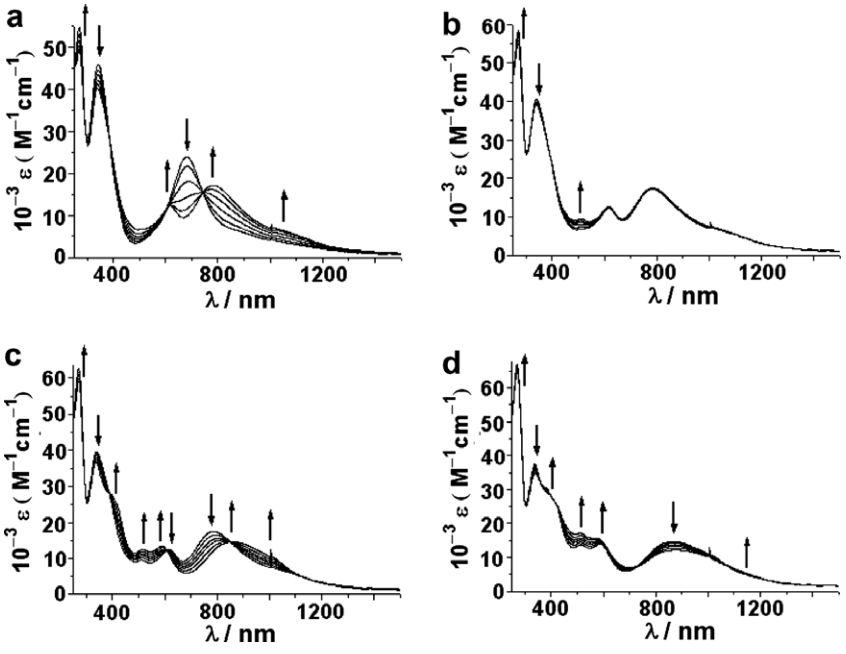

Fig. 10. UV–Vis–NIR spectroelectrochemistry for the conversions: (a) $\mathbf{1} \rightarrow \mathbf{1}^{-}$, (b) $\mathbf{1}^{-} \rightarrow \mathbf{1}^{2-}$, (c) $\mathbf{1}^{2-} \rightarrow \mathbf{1}^{3-}$ and (d) $\mathbf{1}^{3-} \rightarrow \mathbf{1}^{4-}$ in CH_3CN/0.1 M Bu_4NPF_6.

Table 5
UV–Vis–NIR data for complexes **1** and **2** from spectroelectrochemistry[a]

Complex	λ_{max} (nm) (ε, M^{-1} cm^{-1})
$\mathbf{1}^{3+}$	687 (18300), 440 (30000), 366 (38700), 290 (38600), 247 (52000)
$\mathbf{1}^{2+}$	865sh, 700sh, 602 (16800), 438sh, 362 (40900), 275sh, 248 (48400)
$\mathbf{1}^{+}$	685sh, 620 (18800), 435sh, 350 (43100), 270 (46500), 252 (46900)
1	890sh, 680 (23900), 342 (47600), 271 (50500), 250sh
$\mathbf{1}^{-}$	1060sh, 783 (17200), 616 (12300), 340 (40600), 270 (54900)
$\mathbf{1}^{2-}$	1065sh, 785 (17400), 617 (12500), 511 (9500), 339 (39200), 272 (58600)
$\mathbf{1}^{3-}$	1018 (9800), 865 (14800), 589 (13500), 515 (12600), 410 (27200), 338 (37000), 271 (63000)
$\mathbf{1}^{4-}$	1145sh, 880 (12300), 573 (15700), 512 (17100), 380sh, 340 (34900), 270 (67100)
$\mathbf{2}^{3+}$	618 (7900), 424 (20400), 350 (28900), 289sh, 243 (29400)
$\mathbf{2}^{2+}$	584 (8800), 414 (19100), 347 (29100), 326sh, 276sh, 243 (28500)
$\mathbf{2}^{+}$	614 (10700), 416sh, 334 (29100), 276 (25800), 243 (25300)
2	644 (12100), 331 (30400), 275 (27300), 242 (25700)
$\mathbf{2}^{-}$	723 (9400), 582 (8000), 337 (27400), 275 (28500), 247 (26500)
$\mathbf{2}^{2-}$	840sh, 747 (9500), 546 (7100), 415sh, 336 (25000), 274 (29800), 250sh
$\mathbf{2}^{3-}$	1017 (4700), 861 (8200), 787 (8900), 533 (8200), 411 (15800), 333 (23700), 274 (32600), 256sh

[a] In CH_3CN/0.1 M Bu_4NPF_6.

a situation with several filled d orbitals from three d^6 metal centers and a number of ligand π^* MOs (Fig. 4) there are several other MLCT transitions of lower energy but much smaller oscillator strengths (poor orbital overlap) which are not experimentally detectable (Table S2). A similar reason may preclude [8] the detection of the inter-valence charge transfer (IVCT) bands of the mixed-valent forms $\mathbf{1}^{+}$, $\mathbf{1}^{2+}$, $\mathbf{2}^{+}$ and $\mathbf{2}^{2+}$ in the typical near-infrared region [1,3]. In spite of careful spectral search even in the mid-infrared region we could not establish such bands (Table 5), although $[Ru(bpy)_2]^{2+}$ complexes of the related 1,4,5,8,9,12-hexaazatriphenylene ligands exhibit such features [3b,3c]. This absence of detectable long-wavelength absorption for otherwise clearly identified Ru^{II}/Ru^{III} mixed-valent intermediates has been noted before not only for $\mathbf{3}^{+}$ and $\mathbf{3}^{2+}$;8 dinucleating chelate acceptor bridges connecting ruthenium complex fragments, especially $Ru(acac)_2$, have previously been described to yield "IVCT silent" mixed-valent species [24]. An alternative interpretation [3a] involving the obscuring of the IVCT band by the MLCT absorptions in the visible would imply an usually strong metal–metal interaction which we consider less likely.

Within the spectroelectrochemically monitored electron transfer series (Figs. 9,10, and Table 5) it is remarkable that the second oxidation and reduction involve very little spectral changes. This may suggest spin pairing of the doubly reduced or oxidized forms in agreement with the absence of EPR triplet features. Although they can be generally assigned as MLCT and, at higher energies, as intra-ligand (IL) absorptions, the detailed identification of the major bands of the spectroelectrochemically generated complex ions (Table 5) will not be attempted and will have to await open-shell calculations. Given the photophysical and intercalating potential of such large π systems [25] further investigations of their electronic structures are warranted.

4. Conclusion

We have shown that EPR spectroscopy in conjunction with electrochemistry can provide an alternative way to identify mixed-valent intermediates, especially when the expected inter-valence CT bands in the long-wavelength region are not observable. The six fold substitution of the large heterocyclic π system clearly affects the physical properties, allowing not only for multiple oxidation at the metals but also for several ligand based reduction processes.

Acknowledgements

Financial support received from the Department of Science and Technology (DST), Council of Scientific and Industrial Research (CSIR)-New Delhi (India), the Deutsche Forschungsgemeinschaft (DFG), Fonds der Chemischen Industrie (FCI), the Deutsche Akademische Austauschdienst (DAAD) (Germany), is gratefully acknowledged.

Appendix A. Supplementary material

Supplementary data associated with this article can be found, in the online version, at doi:10.1016/j.poly.2007.03.030.

References

[1] (a) C. Creutz, Prog. Inorg. Chem. 30 (1983) 1;
(b) D.E. Richardson, H. Taube, Coord. Chem. Rev. 60 (1984) 107;
(c) K.D. Demadis, D.C. Hartshorn, T.J. Meyer, Chem. Rev. 101 (2001) 2655;
(d) J.T. Hupp, in: J.A. McCleverty, T.J. Meyer (Eds.), Comprehensive Coordination Chemistry II, Elsevier Science, Amsterdam, 2004, p. 709;
(e) M.D. Ward, Chem. Soc. Rev. 24 (1995) 121;

(f) F.R. Keene, Chem. Soc. Rev. 27 (1998) 185;
(g) G. Giuffrida, S. Campagna, Coord. Chem. Rev. 135 (1994) 517;
(h) K. Kalyanasundaram, M.K. Nazeeruddin, Inorg. Chim. Acta 226 (1994) 213;
(i) D.M. D'Alessandro, F.R. Keene, Chem. Soc. Rev. 35 (2006) 424;
(j) D.M. D'Alessandro, F.R. Keene, Chem. Rev. 106 (2006) 2270;
(k) R.J. Crutchley, in: J.A. McCleverty, T.J. Meyer (Eds.), Comprehensive Coordination Chemistry II, Vol. 2 (2004) 235;
(l) J.-P. Launay, Chem. Soc. Rev. 30 (2001) 386.

[2] K.-I. Ota, H. Sasaki, T. Matsui, T. Hamaguchi, T. Yamaguchi, T. Ito, H. Kido, C.P. Kubiak, Inorg. Chem. 38 (1999) 4070.

[3] (a) B.D. Yeomans, L.S. Kelso, P.A. Tregloan, F.R. Keene, Eur. J. Inorg. Chem. (2001) 239;
(b) D.M. D'Alessandro, F.R. Keene, Chem. Eur. J. 11 (2005) 3679;
(c) D.M. D'Alessandro, M.S. Davies, F.R. Keene, Inorg. Chem. 45 (2006) 1656;
(d) L. Jacquet, A. Kirsch-De Mesmaeker, J. Chem. Soc., Faraday Trans. 88 (1992) 2471.

[4] S. Kar, T.A. Miller, S. Chakraborty, B. Sarkar, B. Pradhan, R.K. Sinha, T. Kundu, M.D. Ward, G.K. Lahiri, Dalton Trans. (2003) 2591.

[5] S. Kar, B. Pradhan, R.K. Sinha, T. Kundu, P. Kodgire, K.K. Rao, V.G. Puranik, G.K. Lahiri, Dalton Trans. (2004) 1752.

[6] N. Shan, S.J. Vickers, H. Adams, M.D. Ward, J.A. Thomas, Angew. Chem. 116 (2004) 4028.

[7] N. Shan, S.J. Vickers, H. Adams, M.D. Ward, J.A. Thomas, Angew. Chem., Int. Ed. 43 (2004) 3938.

[8] S. Patra, B. Sarkar, S. Ghumaan, J. Fiedler, W. Kaim, G.K. Lahiri, Dalton Trans. (2004) 754.

[9] T. Kobayashi, Y. Nishina, K. Shimizu, G.P. Satô, Chem. Lett. (1988) 1137.

[10] G. Kestemont, V.D. Halleux, M. Lehmann, D.A. Ivanov, M. Watson, Y.H. Geerts, Chem. Commun. (2001) 2074.

[11] V.J. Catalano, W.E. Larson, M.M. Olmstead, H.B. Gray, Inorg. Chem. 33 (1994) 4502.

[12] M. Krejcik, M. Danek, F. Hartl, J. Electroanal. Chem. 317 (1991) 179.

[13] W. Kaim, S. Ernst, V. Kasack, J. Am. Chem. Soc. 112 (1990) 173.

[14] (a) M. Dolg, U. Wedig, H. Stoll, H. Preuss, J. Chem. Phys. 86 (1987) 866;
(b) D. Andrae, U. Haussermann, M. Dolg, H. Stoll, H. Preuss, Theor. Chim. Acta 77 (1990) 123;
(c) M.J. Frisch et al., GAUSSIAN 98, Revision A.6, Gaussian, Inc., Pittsburgh, PA, 1998;
(d) C. Lee, W. Yang, R.G. Parr, Phys. Rev. B 37 (1988) 785;
(e) M. Casida, in: D.P. Chong (Ed.), Recent Advances in Density Functional Methods, vol. 1, World Scientific Press, Singapore, 1995, p. 155;
(f) J.E. Monat, J.H. Rodriguez, J.K. McCusker, J. Phys. Chem. 106 (2002) 7399;
(g) S.I. Gorelsky, AOMIX: Program for Molecular Orbital Analysis, York University: Toronto, Canada, 1997. <http://www.sg-chem.net/>;
(h) G. Schaftenaar, J.H. Noordik, J. Comput. – Aid. Mol. Des. 14 (2000) 123.

[15] S. Patra, B. Sarkar, S. Maji, J. Fiedler, F.A. Urbanos, R. Jimenez-Aparicio, W. Kaim, G.K. Lahiri, Chem. Eur. J. 12 (2006) 489.

[16] W. Kaim, B. Olbrich-Deussner, R. Gross, S. Ernst, S. Kohlmann, C. Bessenbacher, in: M. Chanon (Ed.), Importance of Paramagnetic Organometallic Species in Activation, Selectivity and Catalysis, Kluwer Academic Publishers, Dordrecht, 1989, p. 283.

[17] (a) F. Barrière, W.E. Geiger, J. Am. Chem. Soc. 128 (2006) 3980;
(b) D.M. Alessandro, F.R. Keene, Dalton Trans. (2004) 3950;
(c) R.J. Crutchley, Adv. Inorg. Chem. 41 (1994) 273;
(d) C.E.B. Evans, M.L. Naklicki, A.R. Rezvani, C.A. White, V.V. Kondratiev, R.J. Crutchley, J. Am. Chem. Soc. 120 (1998) 13096;
(e) M. Al-Noaimi, G.P.A. Yap, R.J. Crutchley, Inorg. Chem. 43 (2004) 1770.

[18] B. Sarkar, S. Patra, J. Fiedler, R.B. Sunoj, D. Janardanan, S.M. Mobin, M. Niemeyer, G.K. Lahiri, W. Kaim, Angew. Chem. 117 (2005) 5800.

[19] B. Sarkar, S. Patra, J. Fiedler, R.B. Sunoj, D. Janardanan, S.M. Mobin, M. Niemeyer, G.K. Lahiri, W. Kaim, Angew. Chem., Int. Ed. 44 (2005) 5655.

[20] R. Hariram, B.K. Santra, G.K. Lahiri, J. Organomet. Chem. 540 (1997) 155.

[21] W. Kaim, Coord. Chem. Rev. 76 (1987) 187.

[22] S.I. Gorelsky, A.B.P. Lever, J. Organomet. Chem. 635 (2001) 187.

[23] S.I. Gorelsky, A.B.P. Lever, M. Ebadi, Coord. Chem. Rev. 230 (2002) 97.

[24] (a) S. Chellamma, M. Lieberman, Inorg. Chem. 40 (2001) 3177;
(b) See also J. Poppe, M. Moscherosch, W. Kaim, Inorg. Chem. 32 (1993) 2640;
(c) S. Patra, B. Sarkar, S. Ghumaan, J. Fiedler, W. Kaim, G.K. Lahiri, Inorg.Chem. 43 (2004) 6108.

[25] (a) A. Masschelein, A. Kirsch-De Mesmaeker, C. Verhoeven, R.N. Hinkens, Inorg. Chim. Acta 129 (1987) L13;
(b) R. Blasius, C. Moucheron, A. Kirsch-De Mesmaeker, Eur. J. Inorg. Chem. (2004) 3071.